Improvement in the sensitivity of LA-ICP-MS bioimaging by addition of nitrogen to the argon carrier gas

Monique G. Mello[a]*, Thomas E. Lockwood[a]*, Jonathan Wanagat[b], Mika T. Westerhausen[a], David P. Bishop[a]

[a]Hyphenated Mass Spectrometry Laboratory, Faculty of Science, University of Technology Sydney, P.O. Box 123, Broadway, NSW 2007, Australia
[b]Division of Geriatrics, Department of Medicine, David Geffen School of Medicine at UCLA, Los Angeles, CA 90095, USA
*these authors contributed equally
Email. david.bishop@uts.edu.au

Abstract

Elemental bioimaging of low abundant elements via laser ablation-inductively coupled plasma mass spectrometry (LA-ICP-MS) is hampered by a lack of sensitivity. Novel solutions for specific applications have been developed, however there is a need for more universal approaches. Here we investigated the addition of N_2 to the ICP carrier gas to increase sensitivity, defined as signal-to-background, for the majority of biologically relevant elements. A gelatine standard that contained 38 elements across the mass range was ablated with increasing amounts of N_2 added to the carrier gas post-ablation. The results show that while all elements examined had an increase in signal intensity, some elements did not have a resultant increase in signal-to-background. Sc, V, Mn, Fe, and Se all exhibited a reduction in signal-to-background ratios across all N_2 flow rates examined, with the remaining elements experiencing signal-to-background increases from 1.2-7.8x, depending on the N_2 flow rate and element. A compromised optimum N_2 flow rate was determined for the analysis all elements and used to image endogenous elements in a mouse brain, and antibody-conjugated elements in a quadriceps muscle section. These images confirmed that the addition of N2 to the carrier gas increased the signal-to-background of the analysis, improving image resolution for endogenous elements and low abundant analytes used for immuno-mass spectrometry imaging of biomarkers. These findings offer a promising avenue for advancing the capabilities of LA-ICP-MS in bio-imaging applications.

Keywords Signal enhancement, LA-ICP-MS, Gas addition, Mixed carrier gas

Introduction

Laser ablation-inductively coupled plasma-mass spectrometry (LA-ICP-MS) imaging is a powerful analytical technique for the analysis of endogenous trace elements in biological tissue sections.[1, 2] In addition, the combination of metal-antibody conjugation protocols and immunolabelling of tissue sections enables the quantitative localisation of biomolecules using LA-ICP-MS, a technique known as immuno-mass spectrometry imaging (iMSI).[3, 4] LA-ICP-MS is highly sensitive, selective and can analyse multiple targets across a tissue section. However, low-abundant targets still pose a challenge due to low sensitivity, particularly for iMSI, where the most common commercial tag only contains 60 – 120 atoms.[5] The low abundance of certain biomolecules[6] has led to immunolabelling approaches that use signal amplification via a modified DNA-exchange based method named SABER-IMC.[7] This approach, while effective for the selected analytes, is still limited in its application and is not a uniform method to increase sensitivity of all potential analytes, whether endogenous elements or exogenous tags on immunolabels.

Argon is commonly used as the plasma gas for ICP-MS due to its availability, and high first ionisation energy (15.76 eV). A secondary gas, such as nitrogen, can be added to the argon to reduce polyatomic interferences from plasma or matrix, increase signal-to-noise ratios and improve limits of detection

(LODs).[8,9] Nitrogen (N_2) is the most commonly used additional gas due to its low cost and ease of handling. N_2 addition to the plasma or sample carrier gas can change characteristics of the plasma as the higher thermal conductivity of N_2 may increase ionisation.[10] N_2 addition has also be shown to increase plasma stability,[11] reduce matrix interferences,[11,12] increase analyte signal responses,[10] and improve the signal-to-noise.[11] However, N_2 addition can also negatively contribute to a higher concentration of N-based polyatomic species,[12,13] and N_2 may be contaminated with Kr and Xe, providing another source of polyatomic interferences.[14] The addition of N_2 to the Ar carrier gas has been used to increase signal intensity during LA-ICP-MS analysis of geological samples and NIST SRMs. This increase is often attributed to the reduction of oxide levels,[12,13,15,16] elemental fractionation,[17] and mass bias[12,18] for geological and synthetic samples. With N_2 flows between 3 – 10 mL min^{-1}, these increases tend to be 2 – 3 fold over the signal intensities obtained without N_2.[12,15,19,20]

While the addition of N_2 into the carrier gas to improve signal intensity for the analysis of geological and glass samples has been demonstrated, its impacts in the field of bioimaging remains unexplored. Here we assessed the potential of N_2 addition to the Ar carrier gas to improve the analysis of endogenous and exogenous elements in tissue sections via LA-ICP-MS. N_2 was added to the carrier gas at various flow rates to assess the effects on the limits of analysis for a wide range of elements. Once the optimal N_2 flow rate was determined, it was applied to the analysis of endogenous elements in murine brain, and to a multiplexed iMSI analysis in murine quadriceps.

Experimental

Reagents

1000 µg mL^{-1} standards of selected elements (see Supplementary Table 1) and Seastar Baseline nitric acid (HNO_3) were supplied by Choice Analytical (Thornleigh, New South Wales, Australia). Tris-HCl (pH 7.4), ethylenediaminetetraacetic acid (EDTA; 10 mM), polyethylene glycol (M_n 400), and gelatine from bovine skin (100 mg; type B) were purchased from Sigma-Aldrich (Castle Hill NSW, Australia).

The list of antibodies is provided in Supplementary Table 2, along with the Maxpar® label they are conjugated with. The anti-dystrophin antibody was conjugated with Maxpar® ^{158}Gd reagent by Standard BioTools (South San Francisco, CA, USA). The remaining antibodies were conjugated in-house with their respective Maxpar® label according to the Standard BioTools protocol. The concentrations of the antibody-conjugates were determined by measuring the absorbance at 280 nm, and as per the protocol were diluted to 0.5 mg mL^{-1} for storage at 4°C. Bloxall blocking solution was purchased from Vector Laboratories (Burlingame, CA, USA), Tween-20 and 10x TBS were obtained from Bio-Rad (Hercules, CA, USA), Richard-Allan Scientific™ Cytoseal™ was sourced from Thermo Fisher Scientific (Waltham, MA, USA).

Murine coronal brain section staining

The murine brain tissue sections were acquired from the Howard Florey Institute of Neuroscience and Mental Health, University of Melbourne, after approval from the Howard Florey Animal Ethics Committee (15-104-FINMH). Briefly, male C57BL/6 mice were raised according to standard animal care protocols and fed normal chow and water ad libitum. An overdose of sodium pentobarbitone (100 mg kg^{-1}) was used to euthanise the animal, and the entire animal was perfused with 30 mL of warmed (37 °C) 0.1 M phosphate buffered saline (PBS), pH 7.4. The tissue was fixed in 4% paraformaldehyde in PBS until the brains sank, after which they were immersed overnight in two changes of 30% sucrose in PBS. The brain tissue was then frozen at -80 °C and mounted in O.C.T.™ via the medulla oblongata and upper spinal cord. After equilibrating at -20 °C, the brains were sectioned using PTFE-coated cryotome blades (DT315R50 Silver Microtome Blades. C. L. Sturkey, Inc., Lebanon PA) 37 on a Cryostar cryotome (CryoStar™, Thermo Fisher Scientific, North Ryde, NSW, Australia) to 30 µm thickness at 90 µm intervals and mounted on standard microscope slides.

Immunolabelling

Human muscle biopsies were obtained with informed consent from adult subjects without muscle disease at the Center for Duchenne Muscular Dystrophy at the University of California Los Angeles under an IRB-approved protocol (#11-001087). Skeletal muscle biopsies from the vastus lateralis were embedded in OCT, frozen in liquid nitrogen, sectioned at 10 µm and stored at -80 °C. The multiplexed human quadriceps sections were air-dried for 30 min, washed twice with 1 x tris-buffered saline (TBS) and incubated with Bloxall blocking reagent for 10 min. After blocking, the sections were washed with TBS (0.1% Tween-20), and incubated with a mixed solution of the antibodies (final dilution of 1:750 for each antibody) overnight at 4 °C. The samples then underwent dehydrated with a series of ethanol washes and coverslipped with Cytoseal™ mounting media. Two xylene incubations were used to remove the organic mounted coverslips and residual mounting media.

External calibration

External calibration standards were prepared according to a previously validated protocol.[21] Briefly, a multi-elemental mix was prepared in a buffer containing 100 mM Tris-HCl buffer (pH 7.4), 10 mM EDTA and 1% w/w polyethylene glycol in ultra-purified water (18.2 MΩ cm^{-1} at 25 °C, Arium Pro Vf, Sartorius, Goettingen, Germany). Three sets of six 10% gelatine solutions were prepared in the same buffer and spiked with differing levels of a multi-element mix. The gelatine standards were heated to 54 °C until aqueous, vortexed for homogenisation, and pipetted into a 6-well HybriWell on a standard microscope slide before immediate freezing at -80 °C for 5 min. The mould was then removed, and the gelatine standards were dried and stored at room temperature until analysis. An aliquot of each gelatine standard was digested in HNO_3 for characterisation via solution nebulisation ICP-MS. The calculated concentrations of the gelatine standards for all selected elements are shown in Supplementary Table 3.

LA-ICP-MS

An Elemental Scientific Lasers NWR193 laser ablation system (Kennelec Scientific; Mitcham, Victoria, Australia) coupled to an Agilent Technologies 7900 Series ICP-MS (Mulgrave, Victoria, Australia) was used for all experiments, and the instrumental parameters are shown in Table 1. N_2 (purity >99.999%) was added to the Ar carrier gas using stainless steel tubing and a quartz T-junction placed prior to the torch, with flow rates controlled using an APEX AX-MC-20SCCM-D/5M mass flow controller (Scitek; Lane Cove, NSW, Australia). An N_2 flow of 20 ml min^{-1} was added into the ICP-MS for at least 30 minutes at the start of each day to purge and stabilise the system, and a 30-minute equilibration time was used between each N_2 flow rate before analysis.

Laser parameters varied depending on the sample type and resolution required. The laser flux (0.3 mJ cm^{-2}) and frequency (20 Hz) were kept constant. Ablation of matrix matched gelatine standards was performed at a beam diameter of 15 µm and scan speed of 60 µm s^{-1}. Mouse brains were collected with a 50 µm beam diameter at 200 µm s^{-1} and total MS integration time of 0.25 s. Multiplexed muscle images were collected with a 10 µm beam diameter at 20 µm s^{-1} and total MS integration time of 0.5 s.

The Ar carrier gas flow through the laser cell was optimised for each N_2 flow rate by ablating NIST 612 and monitoring the signal of Mn, Y, Ce, Th, and the Th/ThO ratio. The optimal Ar carrier gas/N_2 flow did not decrease the signal of the majority of monitored elements and produced the same or lower oxide ratio (<1%) as the standard conditions that did not include N_2 addition. The matrix-matched gelatine standards were analysed at each Ar/N_2 carrier gas flow for each element selected.

Table 1. ICP-MS parameters for LA-ICP-MS imaging analysis.

ICP-MS								
RF power source	1350 W							
Carrier gas (L min^{-1})	1.1	1.05	1.0	0.95	0.9	0.85	0.8	0.75
N_2 (mL min^{-1})	0	4	6	8	10	12	15	20
Sample depth	4 mm							
Extract lens 1 and 2	4.5 V, -125 V							
Omega bias, lens	-80 V, 13.2 V							
Octopole RF	180 V							
Octopole bias	-18 V							
Collision gas	3.1 ml min^{-1} H_2							
KED	5 V							

Data and image processing

LA-ICP-MS images were visualised using pew2,[22] and element plots were calculated and created using the python library matplotlib.

Results and Discussion

Similar to previous observations,[13, 16, 17] the Ar carrier gas flow had to be reduced as the N_2 flow increased to maximise signal intensity and maintain Th/ThO formation rates when ablating NIST 612 glass. To measure the effect N_2 addition has on the LA-ICP-MS signal, spiked gelatine standards (five concentration points) were ablated at a range of N_2 flow rates. Each concentration point of the gelatine standards was ablated six times for long enough to produce 112 data points for each element. The mean value of these six lines was used for further calculations. The addition of N_2 to the carrier gas in the LA-ICP-MS resulted in signal amplification for all elements examined. Supplementary Figure 1 shows that the signal for the majority of low-mid mass elements (Al – Te) were enhanced at all N_2 flows examined. The signal for the lanthanides and high mass elements, while still enhanced at lower N_2 flows, decreased at higher N_2 flows. Addition of nitrogen did not affect the linear range of the instrument, with no changes for any element (measured as a <1% change in r^2, see Supplementary Table 1 for comparison of 0 and 8 mL min^{-1} N_2) identified at any N_2 flow.

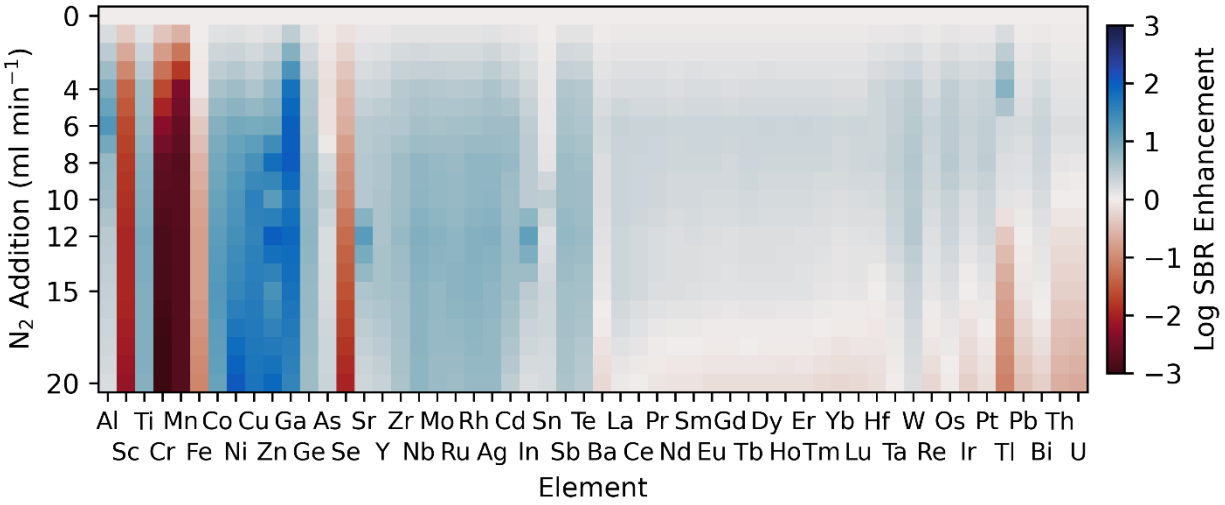

Figure 1. Signal-to-background ratios for measured elements at different N_2 addition flow rates. Values between those measured (0, 4, 6, 8, 10, 12, 15 and 20 ml min^{-1}) are linearly interpolated at a 1 ml min^{-1} step.

Despite the signal enhancement of all elements from nitrogen addition, the formation of N-based polyatomic species can greatly increase background signal.[12, 13] As such, a more important metric is the overall improvement in the signal-to-background ratios (SBRs) of the analysis. SBRs are a common metric in ICP-MS analyses and were used in favour of signal-to-noise ratios due to difficultly in determining noise in the gas-blank for low-noise elements. SBRs were calculated based on the signal of the highest concentration standard divided by the gas blank (Figure 1) at each N_2 flow rate. The majority of elements still show improvements in SBRs, however, some transition metals such as Sc ($^{14}N_2{}^{16}O^1H^+$), V ($^{36}Ar^{15}N^+$, $^{36}Ar^{14}N^1H^+$), Mn ($^{40}Ar^{14}N^1H^+$, $^{40}Ar^{15}N^+$), Fe ($^{40}Ar^{15}N^1H^+$) are prone to N-based polyatomic interferences and, along with Se, had reduced SBRs at all N_2 flow rates.

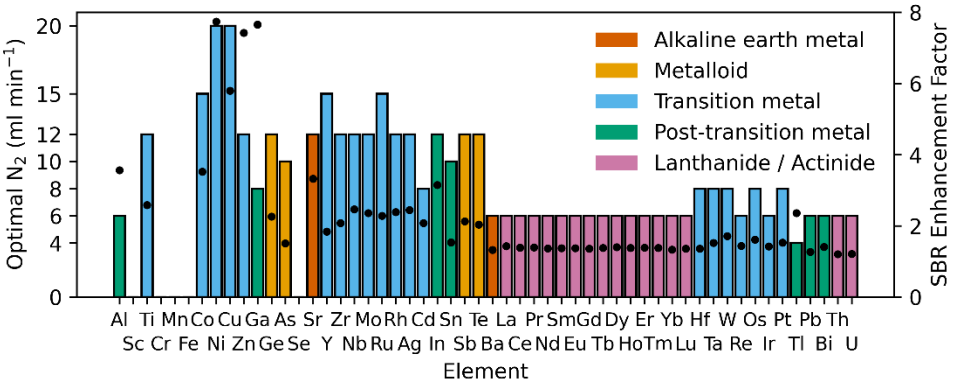

Figure 2. Optimal N_2 addition flow rates (bars) and signal-to-background enhancement factors (dots) for measured elements. Elements are coloured by their group block.

Figure 2 outlines the optimal N_2 flows for the elements that exhibited enhanced SBR. Again, the optimal flow was dependent on the mass. In general, Al – Te required higher flows for optimal SBR enhancement (12 – 20 mL min^{-1}), whereas a lower flow of 6 mL min^{-1} produced best results for the lanthanides and other high mass elements. Transition and post-transition metals benefitted most from nitrogen, with a mean SBR enhancement of 2.8 and 3.0 times. Ni, Cu, Zn and Ga all had >5 times enhancement at their optimal N_2 flows. The lanthanides and the high mass elements exhibited the least enhancement in SBR (<2 times).

The results seen here are consistent with those for the analysis of geological and glass samples by LA-ICP-MS when N_2 was added. We obtained on average a 2 – 3 fold signal-to-background enhancement,[8, 12, 17] and higher levels of enhancement were obtained for the transition elements than the lanthanides and the high mass elements.[8] The majority of elements analysed here exhibited greater enhancement at lower flows, with decreases in signal intensity, and the resultant SBR, of the lanthanides at higher N_2 flows.[10] N-based polyatomics affected the SBR of elements such as V, Cr, and Mn,[12, 13] however the majority of elements experience increases, improving limits of detection (Supplementary Table 6).[15] While some of the increases are modest, these increases could create a notable improvement in image quality and the respective quantitative data extracted when targeting highly complex biological samples with low analyte concentrations of either the element or the biomolecule for iMSI.

Nitrogen addition for the analysis of endogenous elements and metal-conjugated, immunolabelled samples

To show the applicability of using N_2 as a uniform method to enhance the signal-to-background in LA-ICP-MS imaging, nine endogenous elements were measured in a mouse brain section, and ten lanthanides conjugated to antibodies were measured as a proxy for protein abundance in a human quadriceps section. Each analysis involved dividing the section in half, and analysing one half with standard conditions, and the other half with the addition of 8 mL min^{-1} N_2 into the carrier gas. 8 mL min^{-1} N_2 was chosen as a compromise between the optimal values across the entire mass range.

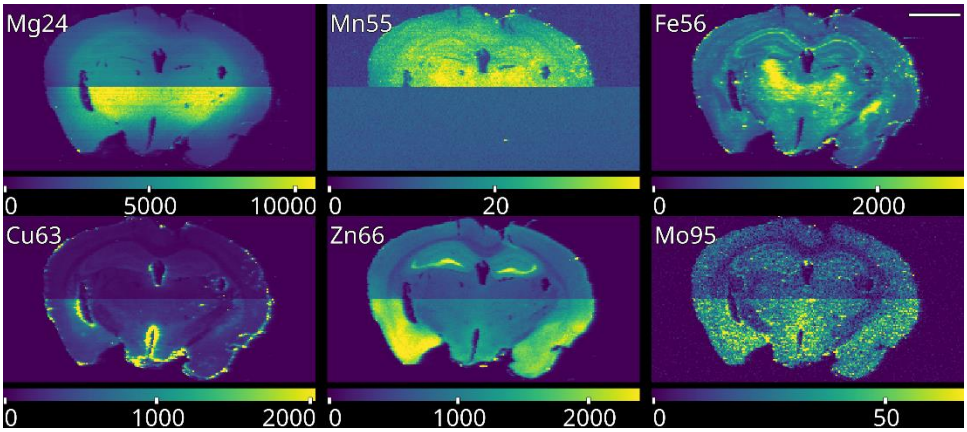

Figure 3. Comparison of the nitrogen addition and standard method for analysing endogenous metals in mouse brain. The top half of each image was collected using standard conditions, and the bottom half with 8 ml min^{-1} nitrogen. Images were formed by dividing the signal collected with the mean background intensity, to show improvements in SBRs. Scale bar is 2 mm and image units signal/background.

Figure 3 shows the comparison of standard conditions vs the addition of N_2 for Mn, Fe, Ni, Cu, Zn and Mo in mouse brain samples (Na, P, and Ni are shown in Supplementary Figure 2). Improvements in SBR are clearly visible for Mg, Cu, Zn and Mo, while Fe is unaffected and all detail in the Mn image was lost. SBR enhancements of 1.9 – 3.5 were measured in the brain tissue, but %RSDs of the mean signal across the section were not affected (Supplementary Table 3). The loss of Mn was expected as Figure 1 demonstrated the large deterioration in SBR, probably due to the increase of the $^{40}Ar^{15}N^{+}$ polyatomic species. Figure 1 also showed that Fe did not have improved sensitivity at any N_2 flow, however the image was not impacted by the slight increase in background due to the high concentrations of Fe present in murine brain.[23] Mo is a low abundant endogenous metal,[24] and the addition of N_2 resulted in a doubling of counts without impacting background signal, improving its detection capacity.

Multiplexed iMSI of ten metal-conjugated antibodies is shown in Figure 4 and Supplementary Figure 3. The majority of these antibodies were conjugated to low-abundant membrane proteins,[25] and as with many iMSI applications,[4, 6, 7, 26, 27] the sensitivity was impacted by the low number of labelled metal atoms per antibody.[5] The addition of N_2 resulted in improved detection capacity, with enhancement ranged from 1.0 to 1.7 times, and %RSDs were unaffected (see Supplementary Table 4). The uniform approach of N_2 addition, while not providing the same levels of improvement in signal response as specific immunolabelling strategies,[7, 26, 27] reduces the complexity of sample preparation and analysis and is a more accessible method.

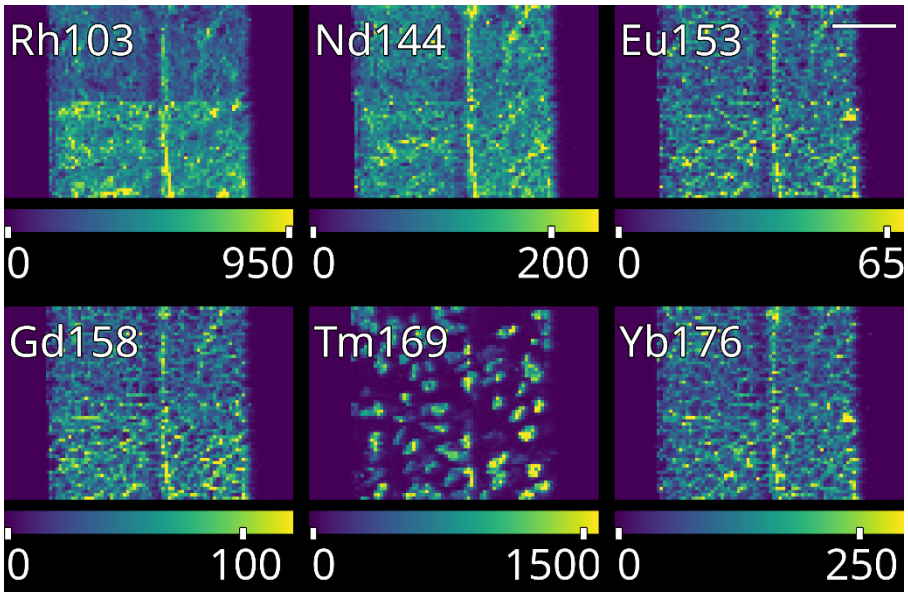

Figure 4. Raw signal for multiplexed imaging of lanthanide tagged antibodies in murine quadriceps muscle tissue sections. The top half of each image was collected using standard conditions and the bottom half with 8 ml min^{-1} nitrogen. Scale bar is 200 µm and the image units are in counts.

Conclusions

Here we have demonstrated that the introduction of N_2 into the argon carrier gas for LA-ICP-MS is a uniform method to improve SBRs for bioimaging applications. The results show that most transition and post-transition metals exhibited an increased signal of 2.8 and 3 times respectively, which did not always translate to improved SBRs with Sc, V, Mn, Fe, and Se experiencing a reduction in SBRs across all N_2 flow rates examined. The lanthanides had mean improvement factors ranging between 1.2 to 1.4 times. While the enhancement in lanthanide signal may seem moderate, it has the potential to substantially contribute to the quantification and resolution of images in complex biological samples characterised by low levels of protein abundance. N_2 was added at 8 mL min^{-1} for the analysis of endogenous elements in murine brain, and a multiplexed iMSI application in human quadriceps. This approach resulted in higher contrast images for the more abundant elements such as Mg, Cu and Zn, in the murine brain, and improved the detection capabilities for lower abundant elements including Mo and lanthanide-conjugated antibodies in iMSI. The use of this uniform approach to improve the SBRs of LA-ICP-MS bioimaging analyses will assist many applications, in particular for low abundant analytes, and will allow for moderate decreases in laser spot sizes to increase image resolution.

Acknowledgements

The authors thank Associate Professor Dominic Hare for supplying the murine brain sections, and Agilent Technologies for the loan of the ICP-MS. DPB was supported by the Australian Research Council Discovery Project grant DP230101740, and JW was supported by National Institutes of Health Grants, R01AG055518, R01AG069924, and K02AG059847.

References

1. D. P. Bishop, D. Clases, F. Fryer, E. Williams, S. Wilkins, D. J. Hare, N. Cole, U. Karst and P. A. Doble, *Journal of Analytical Atomic Spectrometry*, 2016, **31**, 197-202.
2. D. J. Hare, E. J. New, M. D. de Jonge and G. McColl, *Chem. Soc. Rev.*, 2015, **44**, 5941-5958.
3. D. P. Bishop, M. T. Westerhausen, F. Barthelemy, T. Lockwood, N. Cole, E. M. Gibbs, R. H. Crosbie, S. F. Nelson, M. C. Miceli, P. A. Doble and J. Wanagat, *Scientific Reports*, 2021, **11**, 1128.

4. M. Schaier, S. Theiner, D. Baier, G. Braun, W. Berger and G. Koellensperger, *JACS Au*, 2023, **3**, 419-428.
5. S. D. Tanner, D. R. Bandura, O. Ornatsky, V. I. Baranov, M. Nitz and M. A. Winnik, *Pure and Applied Chemistry*, 2008, **80**, 2627-2641.
6. A. von Schoenfeld, P. Bronsert, M. Poc, A. Fuller, A. Filby, S. Kraft, K. Kurowski, K. Sörensen, J. Huber, J. Pfeiffer, M. Proietti, V. Stehl, M. Werner and M. Seidl, *International Journal of Molecular Sciences*, 2022, **23**, 223.
7. T. Hosogane, R. Casanova and B. Bodenmiller, *Nature Methods*, 2023, **20**, 1304-1309.
8. Z. Hu, S. Gao, Y. Liu, S. Hu, H. Chen and H. Yuan, *Journal of Analytical Atomic Spectrometry*, 2008, **23**, 1093-1101.
9. C. Neff, P. Becker, B. Hattendorf and D. Günther, *Journal of Analytical Atomic Spectrometry*, 2021, **36**, 1750-1757.
10. S. F. Durrant, *Fresenius' Journal of Analytical Chemistry*, 1994, **349**, 768-771.
11. D. Beauchemin and J. M. Craig, *Spectrochimica Acta Part B: Atomic Spectroscopy*, 1991, **46**, 603-614.
12. M. Shaheen and B. J. Fryer, *Journal of Analytical Atomic Spectrometry*, 2010, **25**, 1006-1013.
13. H. Louie and S. Y.-P. Soo, *Journal of Analytical Atomic Spectrometry*, 1992, **7**, 557-564.
14. Y. Mitsui, H. Kambara, M. Kojima, H. Tomita, K. Katoh and K. Satoh, *Anal. Chem.*, 1983, **55**, 477-481.
15. Z. Hu, Y. Liu, M. Li, S. Gao and L. Zhao, *Geostandards and Geoanalytical Research*, 2009, **33**, 319-335.
16. T. M. Witte and R. S. Houk, *Spectrochimica Acta Part B: Atomic Spectroscopy*, 2012, **69**, 9-19.
17. Z. Hu, Y. Liu, S. Gao, W. Liu, W. Zhang, X. Tong, L. Lin, K. Zong, M. Li, H. Chen, L. Zhou and L. Yang, *Journal of Analytical Atomic Spectrometry*, 2012, **27**, 1391-1399.
18. S. A. Crowe, B. J. Fryer, I. M. Samson and J. E. Gagnon, *Journal of Analytical Atomic Spectrometry*, 2003, **18**, 1331-1338.
19. T. Iizuka and T. Hirata, *Chemical Geology*, 2005, **220**, 121-137.
20. T. D. F. Leite, R. Escalfoni, T. C. O. da Fonseca and N. Miekeley, *Spectrochimica Acta Part B: Atomic Spectroscopy*, 2011, **66**, 314-320.
21. M. T. Westerhausen, T. E. Lockwood, R. Gonzalez de Vega, A. Röhnelt, D. P. Bishop, N. Cole, P. A. Doble and D. Clases, *Analyst*, 2019, **144**, 6881-6888.
22. T. E. Lockwood, M. T. Westerhausen and P. A. Doble, *Anal. Chem.*, 2021, **93**, 10418-10423.
23. D. Hare, B. Reedy, R. Grimm, S. Wilkins, I. Volitakis, J. L. George, R. A. Cherny, A. I. Bush, D. I. Finkelstein and P. Doble, *Metallomics*, 2008, **1**, 53-58.
24. I. Császma, E. Andrási, A. Lásztity, É. Bertalan and D. Gawlik, *Journal of Analytical Atomic Spectrometry*, 2003, **18**, 1082-1087.
25. S. Murphy, M. Henry, P. Meleady, M. Zweyer, R. R. Mundegar, D. Swandulla and K. Ohlendieck, *Biology*, 2015, **4**, 397-423.
26. R. Rana, R. F. Gómez-Biagi, J. Bassan and M. Nitz, *Bioconjugate Chem.*, 2019, **30**, 2805-2810.
27. Y. Yu, J. Dang, X. Liu, L. Wang, S. Li, T. Zhang and X. Ding, *Anal. Chem.*, 2020, **92**, 6312-6320.